

Figure S1

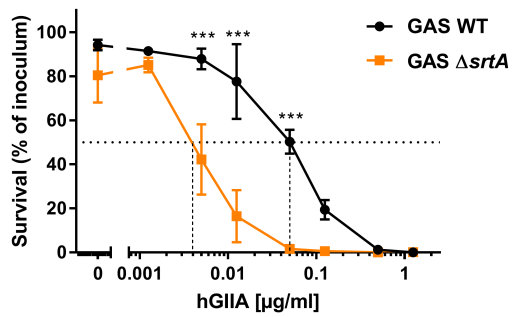


Figure S2

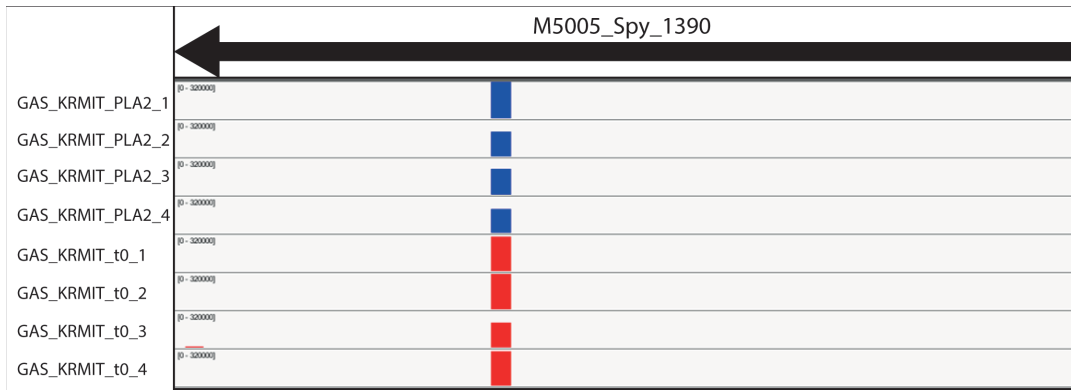


Figure S3

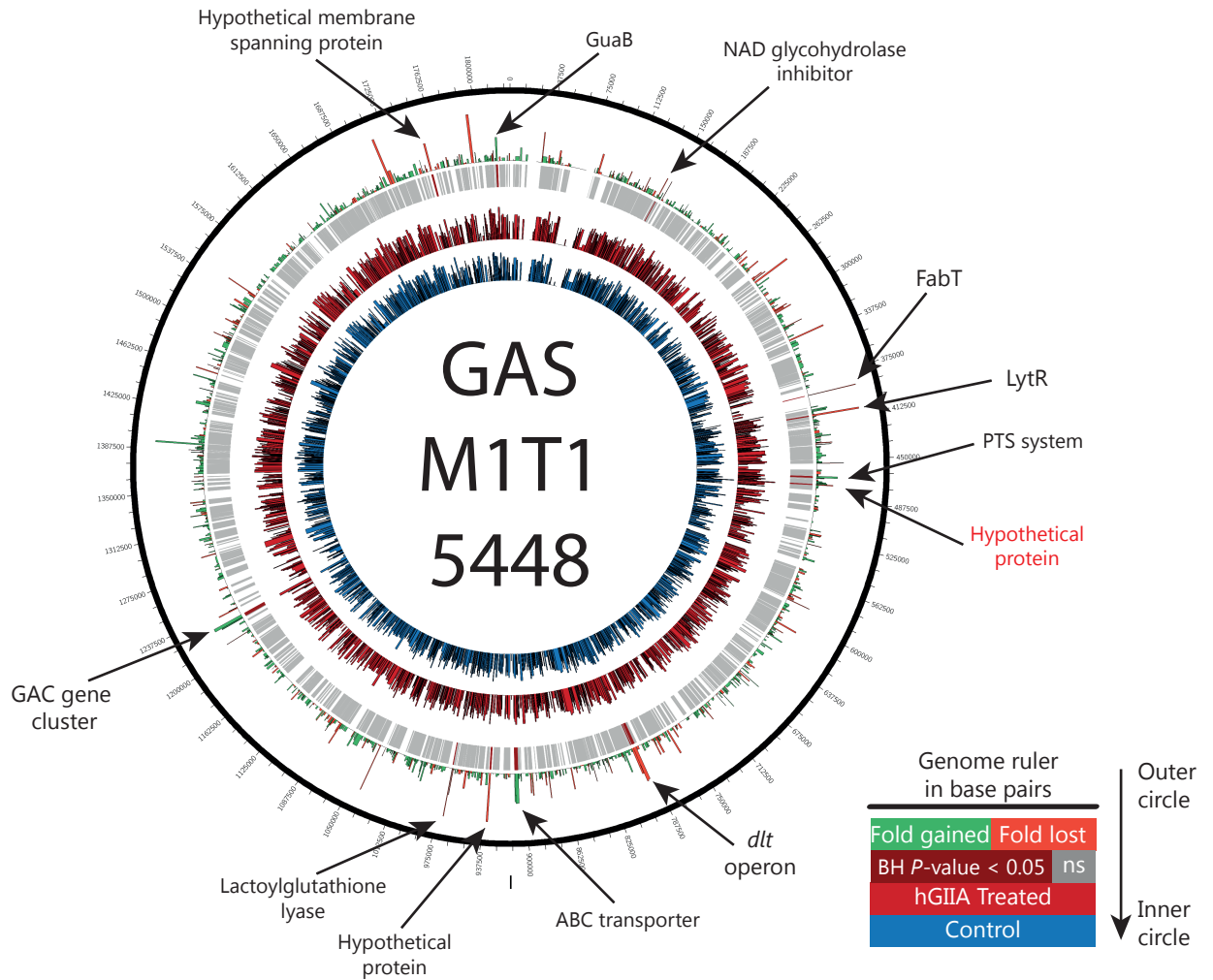


Figure S4

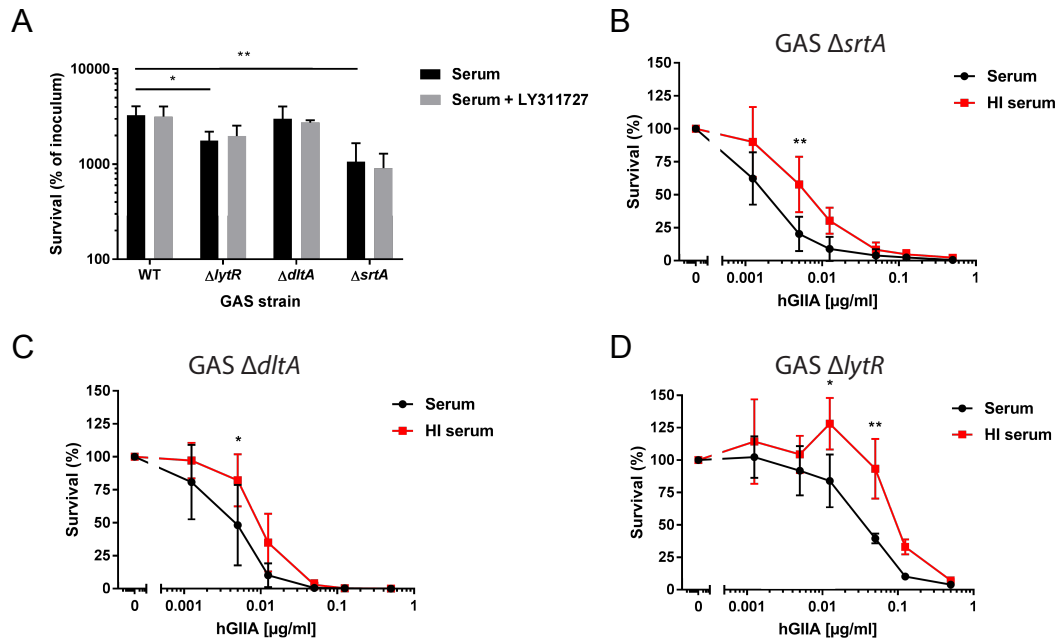


Figure S5

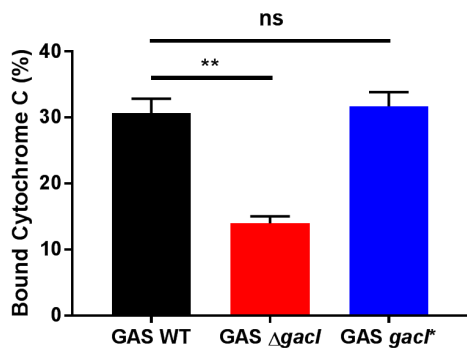


Figure S6

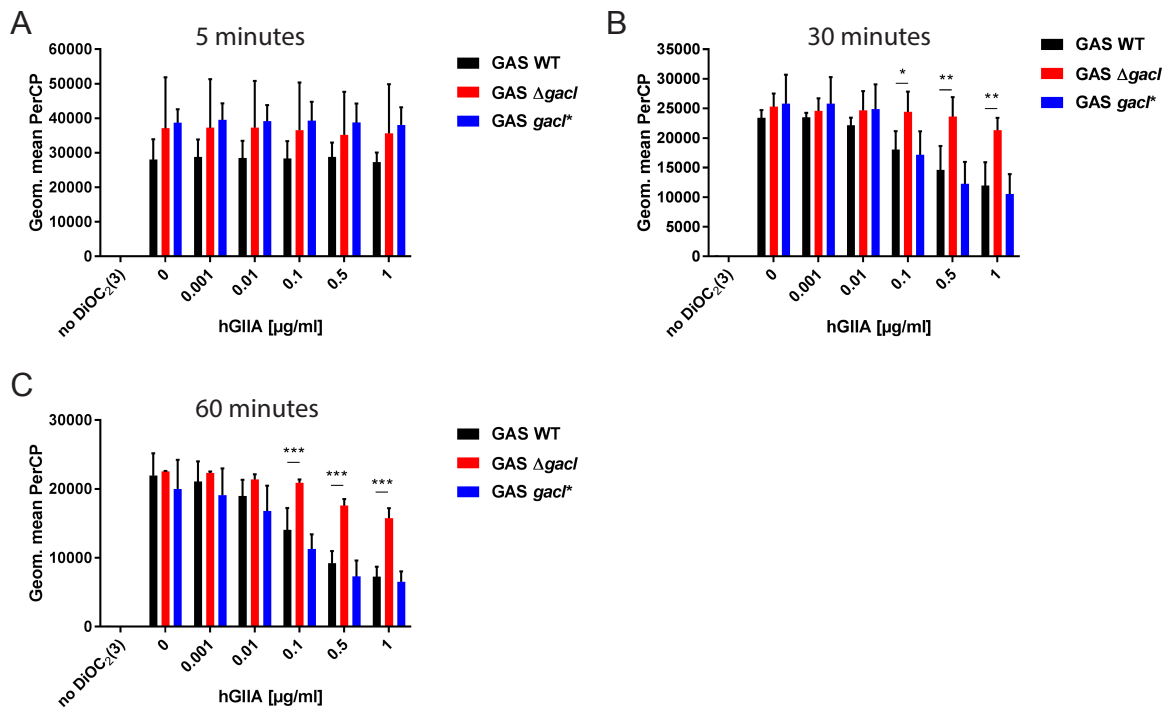


Figure S7

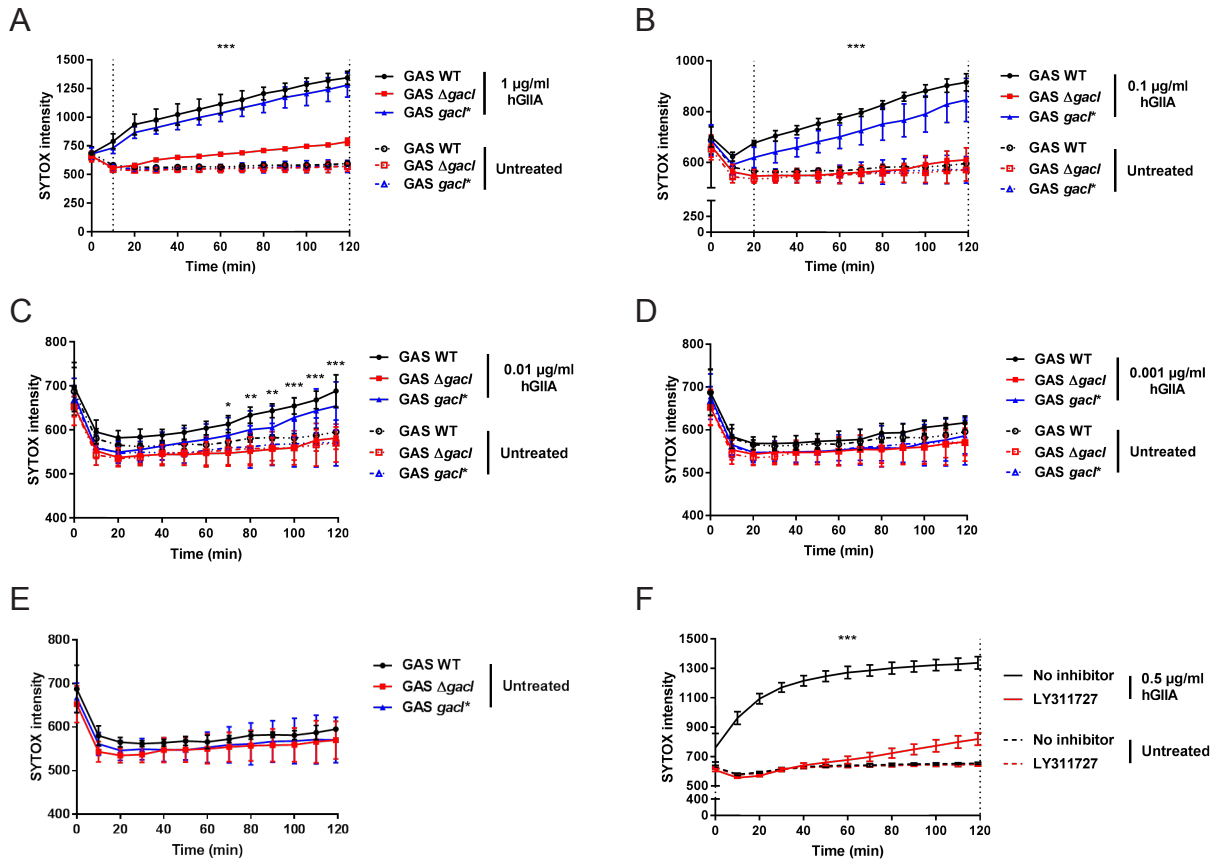


Figure S8

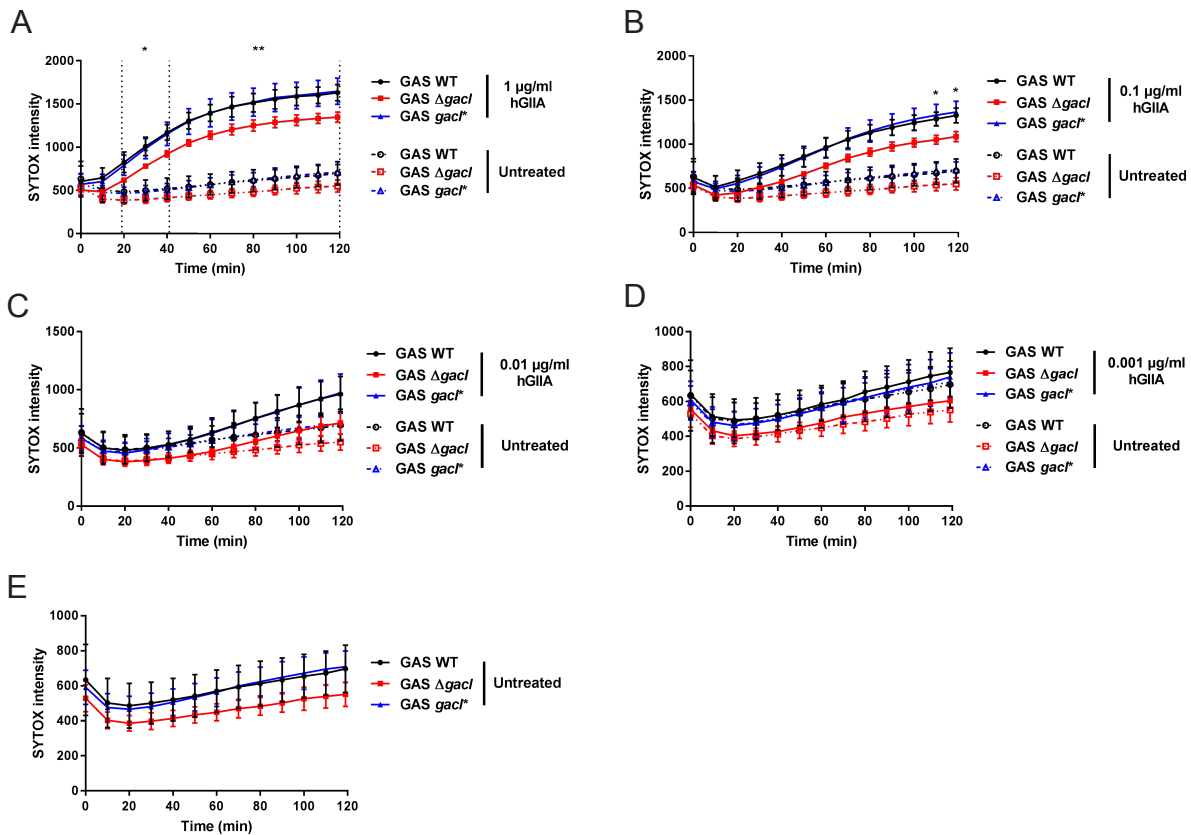
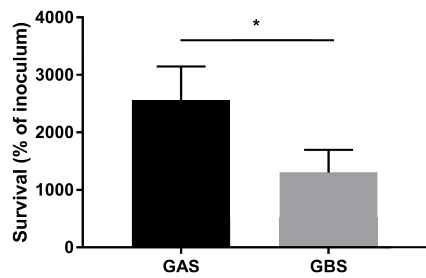


Figure S9

A



B

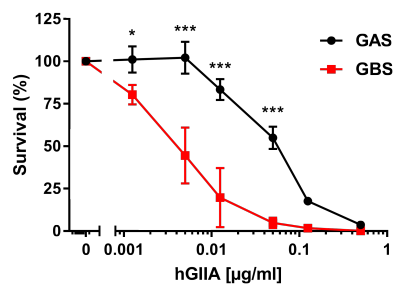


Figure S10

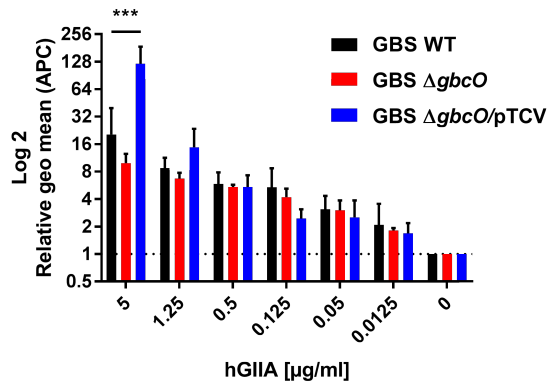


Fig S1. GAS M1T1 5448 is killed by hGIIA in a dose-dependent manner. Mutation of *srtA* renders 5448 more susceptible to hGIIA killing. Data represent mean +/- SD of three independent experiments. ***, $p > 0.001$.

Fig S2. Biased transposon insertions in M5005_Spy_1390. Unusual high number of transposon insertions at one location in the gene M5005_Spy_1390.

Fig S3. Tn-seq results. Circos representation of the Tn-seq data. Each bar in the inner two circles, where blue is control and red the hGIIA treated, represent the average RKPM value of a gene. The following to circles represent the BH corrected p -value and the fold change in log of the hGIIA treated samples vs control samples. Red bars indicate a fold a respective fold decrease and green bars a respective fold increase of transposon insertions. The gene highlighted in red is M5005_Spy_1390, which showed significant fold change due to unusual high transposon insertions at one specific point in the gene.

Fig S4. Serum contains a heat-labile factor that increases hGIIA efficacy. (A) Endogenous hGIIA in serum does not affect growth of GAS. Mutation of *lytR* and *srtA* does attenuate GAS growth independent of hGIIA. This heat-labile factor also affects killing of the (B) *srtA*, (C) *dltA*, and (D) *lytR* mutants. Data represent mean +/- SD of three independent experiments, *, $p > 0.05$; **, $p > 0.01$..

Fig S5. Surface charge of GAS WT and GAS $\Delta gacI$. Deletion of *gacI* affects surface charge of GAS as determined in cationic cytochrome c binding assay. Data represent mean +/- SD of three independent experiments. ns = not significant, **, $p > 0.01$.

Fig S6. Three additional time points for DiOC₂(3) measurements. The effect of hGIIA stress on GAS membrane potential after (A) 5 minutes, (B) 30 minutes and (C) 60 minutes. Data represent mean +/- SD of three independent experiments. *, $p > 0.05$; **, $p > 0.01$; ***, $p > 0.001$.

Fig S7. Kinetics of the SYTOX influx in intact GAS strains. SYTOX influx measured over

120 minutes when GAS strains are incubated with , (A) 1, (B) 0.1, (C) 0.01, (D) 0.001, and (E) 0 $\mu\text{g/ml}$ hGIIA. (F) Addition of 500 μM LY311727 to 0.5 $\mu\text{g/ml}$ hGIIA prevents SYTOX influx. Data represent mean \pm SD of three independent experiments. *, $p > 0.05$; **, $p > 0.01$; ***, $p > 0.001$.

Fig S8. Kinetics of the SYTOX influx in protoplast GAS strains. SYTOX influx measured over 120 minutes when protoplast GAS strains are incubated with (A) 1, (B) 0.1, (C) 0.01, (D) 0.001, and (E) 0 $\mu\text{g/ml}$ hGIIA. Data represents mean \pm SD of three independent experiments. *, $p > 0.05$; **, $p > 0.01$.

Fig S9. Gas and GBS are differently affected by human serum. (A) GAS grows faster in human serum compared to GBS. (B) GBS is more susceptible to hGIIA-spiked in serum compared to GAS. Data represent mean \pm SD of three independent experiments. *, $p > 0.05$; ***, $p > 0.001$.

Fig S10. HGIIA surface binding to GBS. No significant difference in relative hGIIA surface binding of GBS WT and GBS ΔgbcO . Data represent mean \pm SD of three independent experiments. ***, $p > 0.001$.